Arctic Sea Ice Thickness estimation from passive microwave satellite observations between 1.4 and 36 GHz

Clément Soriot[1], Catherine Prigent[1], Carlos Jimenez[3], Frédéric Frappart[2]

[1]LERMA, Paris Observatory, CNRS, PSL, 61 avenue de l'Observatoire, 75014 Paris, France.
[2]Estellus, 93 boulevard de Sebastopol, 75002 Paris, France.
[3]ISPA, INRAE/Bordeaux Sciences Agro, 71 Avenue Edouard Bourlaux, 33140 Villenave D'Ornon, France.

Key Points:

- High correlation is evidenced over the Arctic between passive microwave signatures and SIT derived from lidar and radar altimeters.
- A Neural Network inversion is able to estimate SIT from passive microwave observations.
- The new SIT results show good performances when compared to other satellite or model-derived SIT, as well as to campaign measurements.

Corresponding author: Clément Soriot, `clement.soriot@observatoiredeparis.psl.eu`

Abstract

Arctic sea ice thickness (SIT) have been mostly retrieved from microwaved and visible altimeters since the 2000s. However, the repeatability of altimeters and their spatial coverage limit SIT estimates spatially and temporally. On the other hand, the passive microwave (PMW) radiometer have daily basin-scale coverage of the Arctic. In this study, we proposed a SIT retrieval from PMW observations, based on a statistical inversion technique. It is based on the evidence of hig correlations between PMW observations and existing altimetric satellite-derived SIT, especially at 36 GHz. Lidar ICESat-2 SIT products were used to train a neural network with multiple combinations of brightness temperatures between 1.4 and 36 GHz as inputs over the 2018-2019 time period. The PMW retrieved SIT can mimic the lidar SIT product over the full winter over the Arctic, with a correlation of 0.85, and a RMSE of 0.54 cm. Results were also compared with the altimeter CS2SMOS and the Nucleus for European Modelling of the Ocean (NEMO) SIT products and with the Operation IceBridge QuickLook SIT measurements. The Neural Network (NN) SIT retrieval with all frequencies from 1.4 to 36 GHz has good performance, a correlation of 0.72 and a RMSE of 57 cm when compared to OIB-QL measurements, for large sea ice thickness (mostly above 3 m), under multi-year ice environments. The NN SIT retrieval using only 18 and 36 GHz has also shown satisfactory performances, paving the way for the creation of long time series, these two microwave channels being available since the 1980s.

Plain Language Summary

Arctic sea ice thickness (SIT) have been retrieved from satellite radar and lidar altimeters since the 2000s. However, the altimeter spatial coverage and their repeatability limit the SIT estimates, spatially and temporally. On the other hand, satellite passive microwave radiometers have daily basin-scale coverage of the Arctic. In this study, we proposed to estimate SIT from passive microwave observations, with a statistical inversion technique. It is based on the evidence of a high absolute correlation between existing altimetric satellite-derived SIT, and passive microwave observations, especially at 36 GHz. Lidar SIT products are used to train a neural network with multiple combinations of brightness temperatures between 1.4 and 36 GHz as inputs, over the 2018-2019 time period. Results are compared with other satellite and model derived SIT, as well as with in situ campaign measurements. The new passive microwave SIT retrieval with all frequencies from 1.4 to 36 GHz shows good performance, even for large SIT, under multi-year ice environments. The SIT retrieval using only 18 and 36 GHz also has satisfactory performances, paving the way for the development of long time series, these two microwave frequencies being available from satellite since the 1980s.

1 Introduction

Over the last decades, the Arctic region has experienced climate changes at magnitudes and rates higher than most regions in the world (IPCC report, 2019) leading to a large decrease in sea ice extent (SIE) and thickness (SIT) (Pörtner et al., 2019). Sea ice regulates the energy and mass exchange between the atmosphere and the underlying ocean in the polar regions, and the observed sea ice loss over the last ∼40 years contributed to the warming amplification in the boreal region (e.g., Serreze and Barry (2011); Dai et al. (2019)).

The Sea Ice Extent (SIE) has been extensively monitored from passive microwave satellite observations since the late 70's (e.g., Comiso (1986)), and its decline has been evidenced (e.g., Stroeve et al. (2012); Kwok (2018)). Large-scale satellite estimation of the Sea Ice Thickness (SIT), the other necessary parameter to estimate the sea ice volume change, is more recent, with the advent of the laser altimeter missions (Ice, Cloud and Land Elevation Satellite (ICESat and ICESat-2) (Schutz et al., 2005; Abdalati et

al., 2010)), and radar altimeter missions (e.g., ERS 1 and 2 (S. Laxon et al., 2003), or CryoSat-2 (CS2) (Wingham et al., 1986; S. W. Laxon et al., 2013), see Abdalla et al. (2021) for a review). Because of their nadir geometry, the repeatability of altimeters and their spatial coverage limit SIT estimates spatially and temporally. Both altimetry techniques (laser and radar) estimate a freeboard, i.e., the thickness of the layer protruding above the water level: for the laser altimeters, this layer includes the snow cover and for the low frequency radar, the signal is expected to penetrate the snow layer and reach the sea ice surface. The freeboard estimate is the difference between a measurement above sea ice and another one over open ocean or a lead. The estimation of the total sea ice thickness, including the submerged draft sea ice part, always assumes hydrostatic equilibrium, and an estimation of the snow loading over the sea ice. As a consequence, assumptions have to be made, first on the snow depth and density, often using climatologies (Warren et al., 1999), but also satellite estimates or modeling, and second on the ice and water densities. Long time series of publicly available sea ice thickness products include the ICESat-2 monthly winter product from Petty et al. (2020) data or the CS2 winter product from Tilling et al. (2018). The sensitivity of the radar altimeter estimates is expected to decrease for low sea ice thickness, and passive microwave observations at L-Band (1.4 GHz) from the Soil Moisture Ocean Salinity (SMOS, (Font et al., 2010)) or the Soil Moisture Active Passive (SMAP, (Entekhabi et al., 2010)) missions have been exploited (Kaleschke et al., 2010) and merged with the CS2 estimates for an improved product (CS2SMOS) covering the full range of sea ice thickness, and available on a weekly basis over the winter (Ricker et al., 2014).

Satellite-based SIT estimates have been evaluated and compared. Wang et al. (2016) include ICESat-2, CS2, and SMOS products in their comparison against aircraft and model estimates. Sallila et al. (2019) essentially concentrate on the differences between radar altimeter products derived from CS2. In addition to the intrinsic limitations of the different satellite sensors, estimations of SIT are based on several and different assumptions on the snow loading and the geophysical parameters of the sea ice, which leads to differences between SIT products (Wang et al., 2016; Petty et al., 2020), even when using the same instrument (Sallila et al., 2019).

Satellite passive microwave observations have been extensively exploited to estimate Sea Ice Concentration (SIC and the related SIE), sea ice type, as well as snow depth over sea ice, mainly from 18 and 36 GHz measurements from imagers such as the Advanced Microwave Scanning Radiometers (AMSR) or the Special Sensor Microwave / Imagers (SSM/I) (Comiso, 1995; Comiso et al., 2003; Walker et al., 2006; Markus & Cavalieri, 2009). Thin sea ice thickness is also now routinely estimated from passive microwaves at 1.4 GHz (Kaleschke et al., 2016). However, evaluation of the potential of the passive microwave observations to estimate the sea ice thickness for the full thickness range has not triggered yet much efforts, as passive microwave observations are not expected to penetrate the ice for more than 50 cm, and to be directly sensitive to the thicker sea ice, especially at high frequency (Heygster et al., 2014). Nevertheless, we observed unexpected systematic high correlation at basin-scale between passive microwave observations and existing sea ice thickness, during the full winter (see sections below). Recently, Lee et al. (2021) proposed an estimation of the SIT in the Arctic, from the Advanced Microwave Scanning Radiometer 2 (AMSR2, Imaoka et al. (2012)) frequencies between 6 and 36 GHz, based on the assumed proportionality between the scattering optical thickness at these frequencies within the freeboard and the physical thickness of the freeboard, and a realistic snow depth on sea ice. The relationship between the optical thickness and the ice freeboard is derived from a linear fit with ice freeboard from CS2.

Here, we propose to directly exploit the strong statistical relationship observed between the passive microwave observations and the existing large-scale sea ice thickness estimates, to derive SIT using a machine-learning approach. The motivation is twofold: first to develop a method to produce a robust long-time record of sub-monthly SIT at

basin scale, second to prepare the exploitation of the Copernicus Imaging Microwave Radiometer (CIMR) mission. CIMR (Kilic et al., 2018; Donlon, 2020) is a Copernicus High Priority Expansion Mission first designed to monitor the poles. It will observe from 1.4 to 36 GHz, with a large 7 m antenna to reach 5 km spatial resolution at 18 and 36 GHz. The Copernicus Polar Ice and Snow Topography Altimeter, CRISTAL, another Copernicus High Priority Expansion Mission, will also measure the sea ice thickness, overlying snow depth and ice sheet elevations, owing to a dual frequency altimeter operating at Ku (13.5 GHz) and Ka (36.5 GHz) bands, and synergies between these two CIMR and CRISTAL are encouraged.

A database with observations at CIMR frequencies is built, merging the SMAP observations at 1.4 GHz and the AMSR2 ones at 6, 10, 18, and 36 GHz, to characterize sea ice and snow (Soriot et al., 2022). The statistical analysis between the passive microwave measurements and the SIT estimates are conducted for the ICESat-2 SIT (Petty et al., 2022), for the CS2SMOS SIT (Ricker et al., 2017), and for NEMO (Rousset et al., 2015) modeled SIT. The data and methodology are described respectively in Sections 2 and 3. The machine-learning algorithm is trained on the ICESat-2 SIT. The results and their evaluations are presented in Section 4. Section 5 concludes this study.

2 Data

SMAP and AMSR2 provide brightness temperatures (T_B) from 1.4 GHz (L band) to 89.0 GHz (W band) that include the frequency range (1.4 - 36.5 GHz, from L to Ka bands) that will be observed by CIMR. The satellite-derived SIT are extracted from laser altimetry (ICESat-2) or from a combination of radar altimetry and low frequency passive microwave observations (CS2SMOS). The SIT from the NEMO model is also used (Madec & Team, 2008). Comparisons are conducted with the IceBridge-QL aircraft campaign measurements (N. Kurtz et al., 2013).

All large-scale datasets are extracted over the Arctic Ocean above 55°N, for a complete polar year from November 1, 2018, to October 31, 2019. Data are projected onto the same EaseGrid 2.0 at $\sim$ 12.5 km resolution (Brodzik et al., 2012). The sea ice mask from Ocean and Sea Ice Satellite Application Facility (OSI-SAF) is adopted (Tonboe et al., 2017).

2.1 Passive Microwave Satellite Observations

2.1.1 SMAP

Since January 2015, the NASA SMAP mission observes the Earth at 1.4 GHz at both vertical (V) and horizontal (H) polarizations, from a Sun-synchronous 6 AM/6 PM orbit (Entekhabi et al., 2014). It has a 6 m real aperture antenna that provides a spatial resolution of 40 km. The observing incidence angle is 40°, with a 1000 km swath. Its orbit inclination angle of 98° allows the full coverage of the poles.

We directly use the daily surface T_B at 25 km spatial resolution from L2 product (Meissner et al., 2018) provided by Remote Sensing System (`https://data.remss.com/smap/SSS/V04.0/FINAL/L2C` last access: 9 March 2022). These T_B are corrected for the extra-terrestrial signal, and for the Faraday rotation. Within each grid cell, the SMAP T_B are averaged on a $\sim$ 10-day period (depending on the month, the last 10-day period in the month can be slightly longer or shorter), for each frequency, and polarization.

2.1.2 AMSR2

AMSR2 is a radiometer on board the Japanese polar orbiting satellite GCOM-W, launched in May 2012. It provides observations at 55° incidence angles at 6.9, 7.3, 10.65,

18.7, 23.8, 36.5, and 89 GHz, at both V and H polarizations, with spatial resolution from 48 km at 6.9 GHz to 4 km at 89 GHz. With an inclination angle of 88°, AMSR2 does not observe the Arctic above 88°N. Here, we analyze the frequencies common to the CIMR instrument (noted 6, 10, 18, and 36 GHz hereafter). The Level-1R daily T_B at their native spatial resolution (Maeda et al., 2016) are obtained from the JAXA website (`https://gportal.jaxa.jp`, last access: 9 March 2022).

The EaseGrid 2.0 12.5 km spatial resolution is close to the 10 km spatial sampling of the AMSR2 observations, and to the spatial resolution at 36 GHz (Maeda et al., 2016). Within each grid cell, the AMSR2 T_B are averaged on a $\sim$ 10-day period (depending on the month, the last 10-day period in the month can be slightly longer or shorter), for each frequency, and polarization.

2.2 Satellite-derived Sea Ice Thickness over the Arctic

2.2.1 ICESat-2 SIT

The ICESat-2 L4 monthly gridded sea ice thickness product (Petty et al., 2022) is extracted (`https://nsidc.org/data/IS2SITMOGR4`, last access: 19 April 2022), available during the winter from November to April at a resolution of 25 km. It is based on the laser measurement of the total height of the freeboard (the thickness of the emerged sea ice layer plus the snow cover layer) if sea ice concentration is > 50 %, if height samples are at least 25 km of the coast, and under cloud-free conditions. Hydrostatic equilibrium is assumed for estimating the total SIT from the measured freeboard. Estimates of the snow depth as well as the snow, ice, and water densities are also required. The snow depth and density are simulated from the NASA Eulerian Snow on Sea Ice Model (NEOSIM v1.0) (Petty et al., 2018), modified with an empirical piecewise function to increase the initial model spatial resolution (Petty et al., 2020).

2.2.2 CS2SMOS SIT

The CS2SMOS SIT product combines the CS2 radar altimeter estimates (Ricker et al., 2014; Hendricks et al., 2016) with the passive microwave SMOS observations (Tian-Kunze et al., 2014; Kaleschke et al., 2016). The data can be found at `ftps://smos-diss.eo.esa.int` (last access: 19 April 2022). While CS2 lacks the capability to observe thin ice, SMOS is restricted to ice regimes thinner than $\sim$ 1 m (Ricker et al., 2017).

Unlike ICESat-2, CS2 is considered to measure the ice-only freeboard, as the radar frequency (Ku-band at 13 GHz) is expected to penetrate the snow layer and reach the ice surface. Calculation of the total sea ice thickness relies on the hydrostatic equilibrium, with an estimate of the snow loading along with a snow, ice, and water density estimation. The CS2 SIT uses the snow climatology from Warren et al. (1999), for the snow depth and density. The original Warren climatological snow depth is reduced by 50 % over first-year sea ice N. T. Kurtz and Farrell (2011), where discrimination between first-year and multi-year sea ice type is provided by the satellite-derived OSI-SAF product (Aaboe & Down, 2021). The method to retrieve the thin ice SIT from SMOS T_B at 1.4 GHz is based on a thermodynamic sea-ice model and a one-ice-layer radiative transfer model (Tian-Kunze et al., 2014).

An optimal interpolation scheme is developed to merge the CS2 and SMOS SIT estimates. It is applied to weekly CS2 and SMOS SIT estimates, allowing the estimation of the full SIT range. The product is available from mid-October to mid-April, on a weekly basis, with an initial 25 km spatial resolution.

2.3 NEMO Simulations

The NEMO model is a state-of-the-art modelling framework for research activities and forecasting services in ocean and climate sciences (Madec & Team, 2008). It uses the Louvain-La-Neuve Sea Ice Model 3.6 (LIM3.6) (Rousset et al., 2015).

In this study, the global high-resolution monitoring and forecasting system PSY4V3R1 (Gasparin et al., 2018) is adopted. It is based on version 3.1 of the NEMO ocean model, which assimilates satellite sea ice concentration from the EUMETSAT/OSI-SAF. The PSY4V3R1 NEMO model provides a daily SIT product at 2 km resolution that is averaged on the common 12.5 km EASE grid 2.0.

2.4 Sea Ice Thickness Measurement Campaign

The Unified Sea Ice Thickness Climate Data Record (Lindsay & Schweiger, 2013) aggregates all types of measurements of SIT from airplane and submarines operations, from 1947 to current time. In our time window (11/2018-10/2019), only the Operation IceBridge QuickLook (OIB-QL) data are available (N. T. Kurtz et al., 2013). The measurements are provided by a nadir-looking ground penetration depth radar: the Multichannel Coherent Radar Depth Sounder (MCoRDS), operating at 193.9 MHz (Shi et al., 2010). The differences between radar echoes are directly converted to sea ice thickness.

In April 2019, 125,655 initial points have been measured and grouped to form 50-km clusters (N. T. Kurtz et al., 2012). Over the resulting 88 clusters collected by the OIB-QL campaign during this period, 78 are south of 88.5° and are collocated with the previously described datasets. The mean SIT value and its associated SIT uncertainty is provided for each cluster, and the mean SIT values are located on a map (Figure 1).

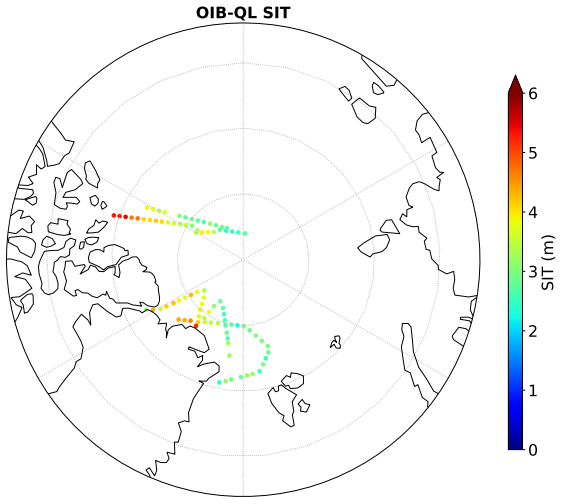

Figure 1. Sea Ice Thickness (SIT) as estimated from the Operation IceBridge QuickLook (OIB-QL) campaign data available for this study, in April 2019.

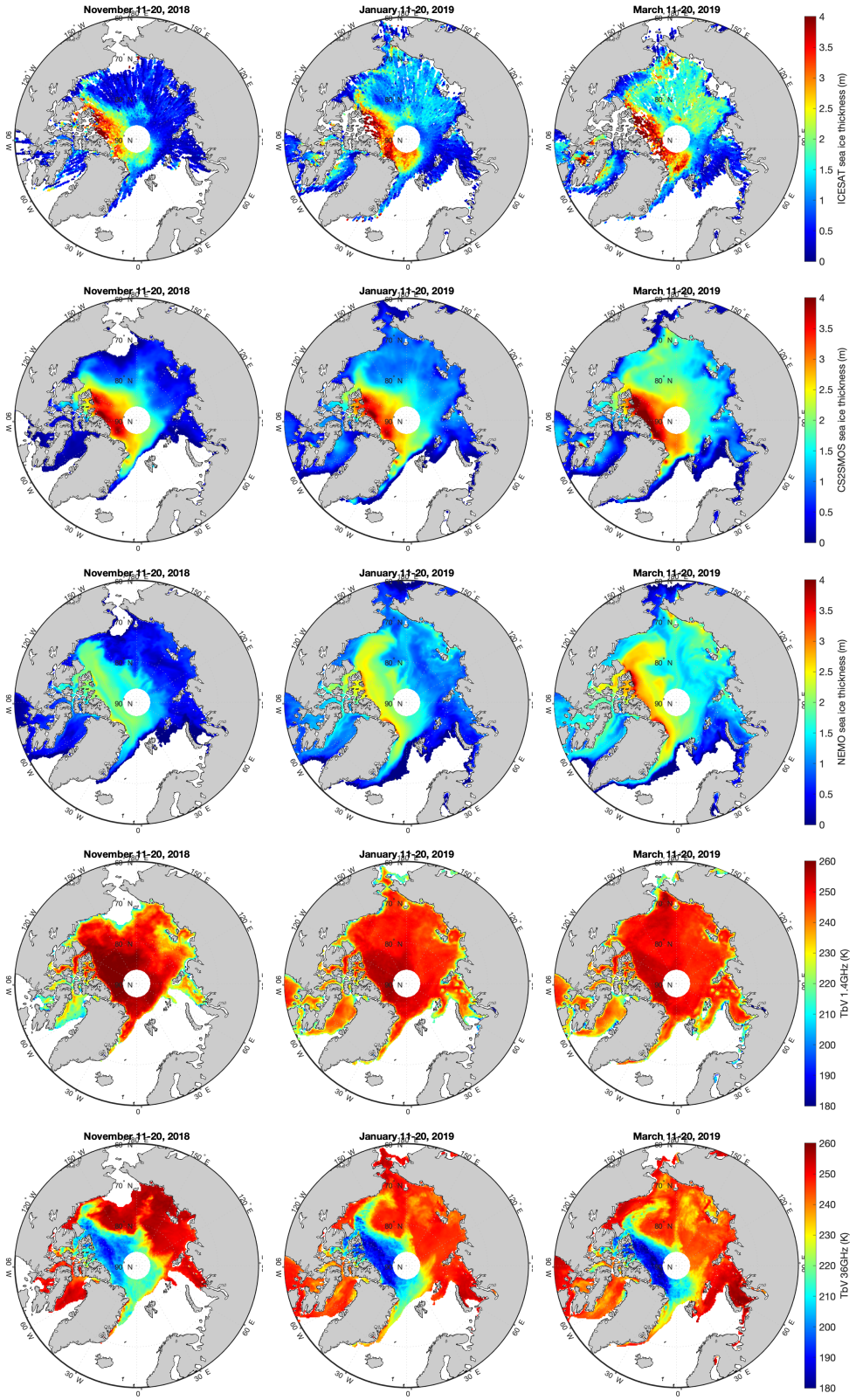

Figure 2. From top to bottom: ICESat-2 SIT, CS2SMOS SIT, NEMO SIT, SMAP T_B^V 1.4 GHz and AMSR2 T_B^V 36 GHz, for three 10-days winter periods (from left to right, the second 10-days periods in November 2018, January 2019, and March 2019), when SIC is above 0.8 (as provided by OSI-SAF estimates).

3 Method

3.1 Preliminary Analysis of the Data

Figure 2 shows, for the second 10-day period of November, January, and March, the SIT from ICESat-2, CS2SMOS, and NEMO as well as the V-polarized brightness temperature T_B^V at 1.4 GHz (SMAP) and 36 GHz (AMSR2), when the OSI-SAF SIC is above 0.8. SIT products from ICESat-2, CS2SMOS, and NEMO show similar broad spatial patterns, although NEMO exhibits significantly less high SIT north of Greenland and the Queen Elizabeth Islands than the satellite estimates. NEMO underestimates the large SIT compared to the other products, and CS2SMOS tends to show lower SIT than ICESAT-2 for these large SIT values as well. The sea ice emissivity at 1.4 GHz is high, and that translates in the maps into high T_B^V (>240 K), with a decrease of T_B^V in areas where sea ice is likely thin and transparent enough for the underneath ocean to contribute to the signal with its low emissivity. The T_B^V maps at 36 GHz exhibit spatial patterns similar to the sea ice thickness derived from the satellites, with a significant decrease of the T_B^V with increasing SIT.

To quantify theses spatial relationships, Figure 3 presents the linear correlation between the SIT from ICESat-2, CS2SMOS, and NEMO, as well as the correlation between the ICESat-2 SIT and T_B^V as a function of time during winter, for selected microwave channels. While the 1.4 GHz T_B^V shows limited correlation with the SIT and the 6 GHz T_B^V shows almost no correlation, there is a strong anti-correlation between the ICESat-2 SIT and T_B^V, at 18 and 36 GHz.

High negative correlation between T_B^V at 18 and 36 GHz and the other SIT products (CS2SMOS and NEMO) is also observed (not shown), with particularly high negative correlation between CS2SMOS and T_B^V at 18 and 36 GHz (above 0.9 in absolute value during the full winter). The spatial linear correlations have also been calculated for two SIT ranges, with a threshold at 0.7 m (not shown). For thin ice below 0.7 m, the correlation between T_B^V at 1.4 GHz and the CS2SMOS SIT is higher than with the other SIT products (ICESat-2 and NEMO). This behavior can be related to the use of T_B at 1.4 GHz in the CS2SMOS product, for its expected sensitivity to the thin ice thickness.

The physical interpretation of this anti-correlation between the T_B^V at higher frequencies and the SIT is not straightforward. These frequencies are not expected to sound within the snow and sea ice. A strong decrease of T_B with increasing frequency is a sign of scattering processes in the radiative transfer (Ulaby & Long, 2014; Soriot et al., 2022). In these regions of low T_B at 18 and 36 GHz, the microwave signal is likely scattered, within the snow pack (volume scattering due to the formation of depth hoar for instance), and possibly as well at the surface (surface scattering), as these regions also correspond to multi-year ice areas, where snow accumulates and where rafting and ridging occur. The relationship between T_B and SIT is likely to bevery indirect, but it is still strong and, as a consequence, it can be potentially exploited for SIT estimation. Given the complexities of emission and scattering processes within the sea ice and snow pack, this is not an uncommon situation and these frequencies (namely 18 and 36 GHz) have already been extensively used to estimate snow depth over sea ice as well as sea ice type (first-year of multi-year), without a robust and clear physical explanation of the direct link between the observation and the snow and ice parameter of interest (see for instance (Rostosky et al., 2018)).

3.2 Statistical Inversion

Given the statistical relationships observed between T_B and SIT, a statistical inversion is tested, based on Neural Network (NN) techniques. NNs have already been widely used in satellite remote sensing for the retrieval of a large number of geophysical parameters, including sea ice variables (Rösel et al., 2012; Braakmann-Folgmann & Donlon,

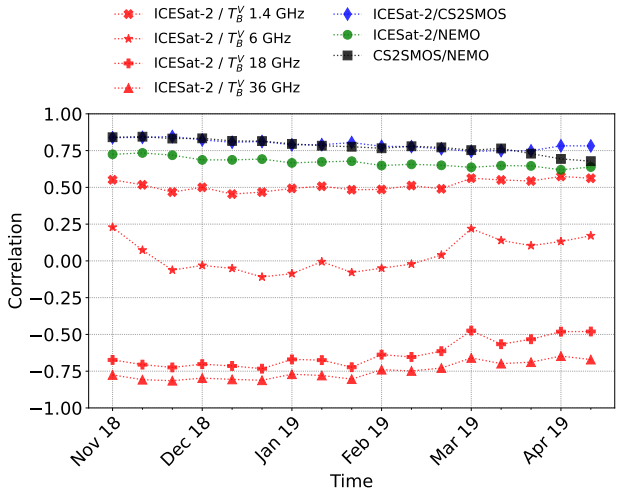

Figure 3. Spatial linear correlation among SIT and between ICESat-2 SIT and selected T_B (1.4, 6, 18, 36 GHz), as a function of time during winter in the Arctic, when SIC is above 0.8 (as provided by OSI-SAF estimates).

2019; Chi & Kim, 2021). Here we adopt a specific NN architecture called Multi Layered Perceptron (MLP) (Rumelhart et al., 1985). The MLP is appropriate to approximate multivariate non-linear mappings (Krasnopolsky, 2007; Cybenko, 1989; Aires et al., 2002), and it will be applied here to build the statistical model reproducing the mapping between brightness temperatures and SIT. The MLP will contain a first layer with as many input neurons as microwave channels used in the retrieval, followed by a hidden layer with tansig activation functions, and an output layer with a linear activation functions and one node outputting the retrieved SIT. This NN architecture can be represented by a function:

$$y_q = a_{q0} + \sum_{j=1}^{k} + a_{qj} \cdot tanh(b_{j0} + \sum_{i=1}^{n} b_{ji} \cdot x_i); q = 1, 2...m \quad (1)$$

where x_i and y_q are components of the NN input and output vectors respectively, and a and b are the matrices of the fitting parameters, i.e, the NN weights and biases. They will be determined during the training phase using a database of brightness temperatures and corresponding SIT, togehter with the training algorithm of (Foresee & Hagan, 1997). To avoid spatial or temporal overfitting and increase the robustness of the retrieval, only a random third of the database will be used for the training, as in Rodríguez-Fernández et al. (2019), and an early-stop validation technique will be applied during the training (Prechelt, 2012).

The NN is trained on the ICESat-2 SIT, to minimize the inbreeding with the passive microwave T_B inputs. The ICESat-2 SIT is expected to be independent of passive microwave observations (Petty et al., 2020) and is retrieved from a different frequency domain (visible versus microwave) (Abdalati et al., 2010). Indeed, the CS2SMOS product is constructed with T_B at 1.4 GHz from SMOS (Ricker et al., 2017), and the NEMO model assimilates OSI-SAF SIC which is based on microwave T_B. However, similar exercise could be performed with a NN trained on CS2SMOS or NEMO. In order to minimize the SIC influence, the NN is trained on pixels with SIC>0.8, as estimated from OSI-SAF.

Several combinations of brightness temperatures have been tested as inputs to the NN and the results are compared with the SIT estimates from CS2SMOS, NEMO, and OIB-QL. Among the tested T_B combinations, two are particularly interesting for further studies: the combination of all CIMR frequencies (1.4, 6, 10, 18 and 36 GHz at both V and H polarizations) to showcase the future capability of CIMR to estimate SIT, and the combination of only 18 and 36 GHz V and H channels, to facilitate the production of long time series of SIT (because of the availability of long-time records of these observations, with SSM/I, its successor SSMIS, and possibly its ancestor, the Scanning Multichannel Microwave Radiometer (SMMR)).

4 Results and Discussion

4.1 Global Arctic Results over the Winter

First, a NN inversion is trained on a subset of the ICESat-2 SIT product, using all the frequencies from the CIMR-like database, from 1.4 to 36 GHz (named PMW_{CIMR} hereinafter). Over the Arctic winter, the linear correlation between the retrieved SIT and the ICESat-2 product is 0.85, with a Root Mean Square Error (RMSE) of 0.54 m.

Figure 4 shows some statistical analyses comparing the different SIT products, including the PMW_{CIMR} retrieval: the spatial linear correlation between the different SIT products as a function of the time (top panel), the RMSE in meter between the different products and the PMW_{CIMR} retrieval as a function of time (middle panel), or as a function of the ICESat-2 SIT (bottom panel). The normalized distribution of the ICESat-2 SIT is also shown in grey shades on the bottom panel.

The general agreement between the satellite products ICESat-2 and CS2SMOS is better (both in terms of spatial correlation and RMSE) than between the satellite products and the NEMO SIT estimates (Figure 4 top panels), as already expected from Figure 2. The agreements are rather stable during the winter, with a slight degradation (decreased correlation and increased RMSE) at the end of the winter season (Figure 4 two top panels). The PMW_{CIMR} retrieval using all frequencies shows better spatial correlation and smaller RMSE with all SIT products at each time step (Figure 4 two top panels, symbols with solid lines), as compared to the initial correlation and RMSE between the ICESat-2 original product and the other SIT products (Figure 4 two top panels, symbols without solid lines). Note that the spatial correlation between PMW_{CIMR} and CS2SMOS SIT is even higher than the correlation between PMW_{CIMR} SIT and the original ICESat-2 SIT used to train it, meaning that the passive microwave information in the PMW_{CIMR} retrieval adds to the agreement between the existing SIT estimates.

The RMSE between products tend to significantly increase between most products, for SIT above $\sim$ 2 m (Figure 4 bottom panel). The SIT population above 2 m is rather limited for all SIT products (the ICESat-2 SIT distribution is indicated in grey shades on Figure 4). For the full SIT range, and especially for the lower and higher SIT, the RMSE between the PMW_{CIMR} retrieval and the other products decreases (symbols with solid lines on Figure 4 bottom panel) as compared to the initial RMS error between ICESat-2 and the other products (symbols without solid lines on the same panel).

Figure 5 shows the maps of the PMW_{CIMR} SIT and the difference between its estimates and the ICESat-2-based SIT estimates for three different 10-days winter periods (11/2018, 01/2019, and 04/2019) not used in the NN training. The maps of the ICESat-2 SIT were already shown (Figure 2). The PMW_{CIMR} SIT maps show the same general patterns as seen in Figure 2, with high SIT north of Greenland and in the Canada Basin, with an increase of the SIT over the winter in the Chukchi Sea. Noticeable differences between PMW_{CIMR} and ICESat-2 SIT are located along the east coast of Greenland, especially in January, where PMW_{CIMR} exhibits higher SIT values than ICESat-2. In this region, note that both CS2SMOS and NEMO have SIT larger than the ini-

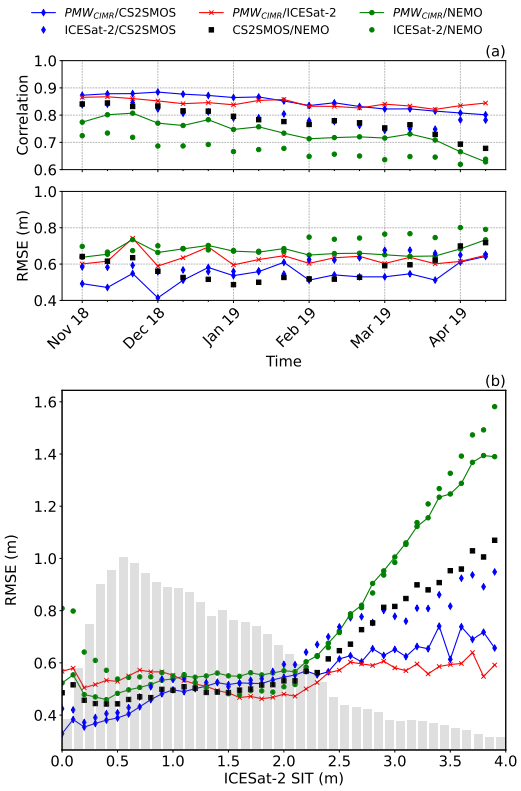

Figure 4. Statistics for inter-prodcut differences, including the PMW_{CIMR} retrieval. Top: Spatial linear correlation (R) between PMW_{CIMR} estimates as a function of time in the winter. Middle: RMSE in m between the variables, also as a function of time in the winter. Bottom: the RMSE between the SIT estimates, as a function of the ICESat-2 SIT (with the ICESat-2 SIT distribution indicated in grey shades).

tial ICESat-2, and closer to the PMW_{CIMR} retrieval (Figure 2). North of the islands of Novaya Zemlya, especially in March, the PMW_{CIMR} predicts higher SIT than ICESAT-2, where also both CS2SMOS and NEMO have higher SIT than ICESat-2. On the contrary, PMW_{CIMR} shows thinner SIT than ICESat-2, in the Bering Strait in January.

The SIT retrieval has also been tested using less frequencies in the training of the NN. Suppressing only the 1.4 GHz channels in the NN does not change much the results (not shown): the correlation with ICESat-2 over the full winter decreases from 0.85 to 0.83, and the RMSE increases from 0.54 m to 0.57 m. It tends to degrade the retrieval of small SIT (<1 m), as compared to the original ICESAT-2 SIT, and to the CS2SMOS SIT, as expected, but only slightly.

Tests are then performed using only the 18 and 36 GHz channels (both V and H polarizations), named PMW_{1836} hereinafter. With this combination, longer SIT time series could be producted, using previous radiometers such as SSM/I (launched in 1987), its successors SSMIS, or even SMMR (launched in 1978) that all include the 18 and 36 GHz channels. The results are presented in Figure 6. The correlation between PMW_{1836} and ICESat-2 SIT decreases over the full winter (from 0.85 with all channels to 0.80 using only 18 and 36 GHz channels), and the RMSE increases (from 0.54 m to 0.62 m), suggesting that the retrieval using only two frequencies would slightly degrade the SIT re-

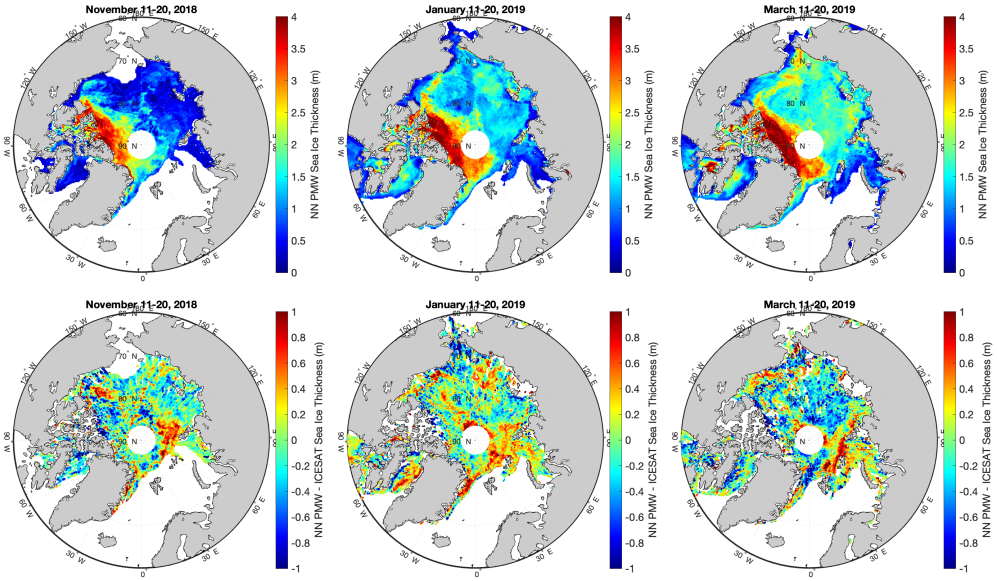

Figure 5. From top to bottom: maps of PMW_{CIMR} SIT, and PMW_{CIMR} SIT minus ICESat-2 SIT, for the PMW_{CIMR} retrieval. For 10-days periods in November 2018 (left), January 2019 (center), and April 2019 (right).

sults compared to the use of all the frequencies available on CIMR, at least when considering ICESat-2 as the reference.

However, surprisingly, compared to CS2SMOS, the correlation and the RMSE do not change much when using all frequencies or 18 and 36 GHz only, with even a slight increase of the correlation (from 0.85 with the CIMR frequencies to 0.88 with only the 18 and 36 GHz channels) and a slight decrease of the RMSE when suppressing all the lower frequencies (from 0.58 m with the CIMR frequencies to 0.54 m with only the 18 and 36 GHz). An explanation could be related to the use of the passive microwave 18 and 36 GHz channels in the CS2SMOS retrieval, for the estimation of the snow depth. Indeed, the CS2 altimeter data processing involves passive microwaves T_B at 18 and 36 GHz to modify the original Warren (Warren et al., 1999) snow depth climatology, following the N. T. Kurtz and Farrell (2011) method. To overcome the need for external snow depth information, future altimeters such as CRISTAL (Kern et al., 2020) will be equipped with dual-frequency radar altimeters, with the snow depth estimation being derived from the difference between the signals at Ku (13 GHz) and Ka (35 GHz) frequencies. Garnier et al. (2021) already tested this possibility for snow depth and SIT retrievals with encouraging results, using two different altimetric missions, CS2 at 13 GHz and SARAL/AltiKa at 35 GHz (Verron et al., 2015). With SARAL/AltiKa limited to 82°N (thus excluding most of the multi-year ice), we did not consider this product in the current comparison.

4.2 Evaluation with the IOB-QL Campaign Measurements

The PMW_{CIMR} estimates are now evaluated with the OIB-QL campaign measurements. Figure 7 shows the results of the comparison between the OIB-QL SIT measurements with the satellite and model retrievals, including the NN retrieval PMW_{CIMR} using all the frequencies from 1.4 to 36 GHz. The clusters were organized by increasing OIB-QL SIT measurement, and their location is provided for each cluster. For each OIB-QL cluster, the mean OIB-QL SIT is shown with its associated uncertainty (red crosses

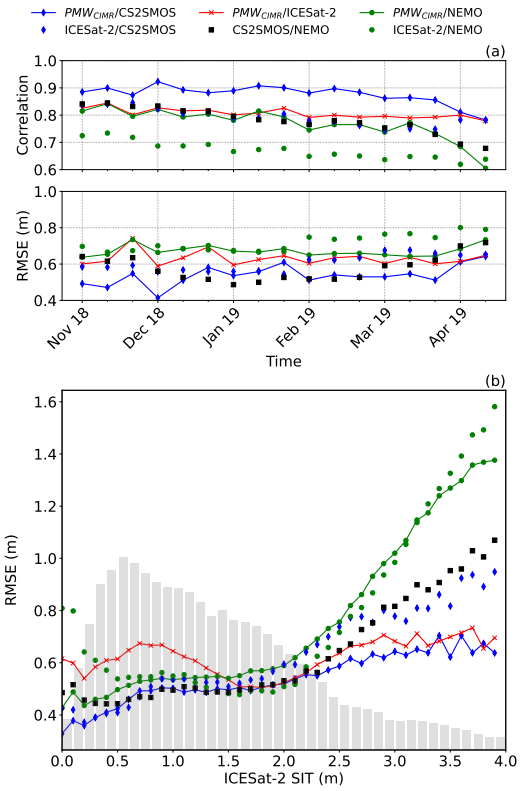

Figure 6. Same as Figure 4, but using the PMW_{1836} retrieval.

and error bars). For the same clusters, the mean SIT retrieved (crosses) and their associated standard deviation (error bars) are shown for PMW_{CIMR} in black, ICESat-2 in green, CS2SMOS in orange and the NEMO model in blue. The normalized distribution of the ICESat-2 SIT is also shown in grey shades.

The range of SIT measured by the OIB-QL campaign shows that most of the sea ice observe is multi-year, with the OIB-QL cluster in the tail of the distribution of the ICESat-2 SIT. CS2SMOS and NEMO show small range of SIT, which can be explained by the fact that these products are spatially smooth (see Figure 2), with consequently few variations over a flight. The NEMO model tends to systematically underestimate the SIT, compared to the measurements campaign, as well as compared to the satellite retrievals.

Table 1 shows the bias, the RMSE, the relative RMSE (in relation to the OIB-QL measurements), and the linear correlation coefficient, between the OIB-QL SIT and the others SIT retrievals (including PMW_{1836}). PMW_{CIMR} shows rather good agreement with the OIB-QL measurements with linear correlations of 0.72, a bias of 16 cm, and a RMSE of 57 cm. The differences between PMW_{CIMR} and PMW_{1836} results are rather limited,considering that 10 channels are used in the first algorithm and only 4 in the second. The CS2SMOS SIT product shows the best agreements with OIB-QL measurements with low mean bias of 11 cm, a RMSE of 49 cm, and a high correlation of 0.8. The PMW_{CIMR} SIT performs slightly better than the ICESat-2 product. NEMO tends to underestimate the OIB-QL values, with a mean bias nearly three times higher than the next worst result (PMW_{1836}), and a RSME nearly two times more important than the other products.

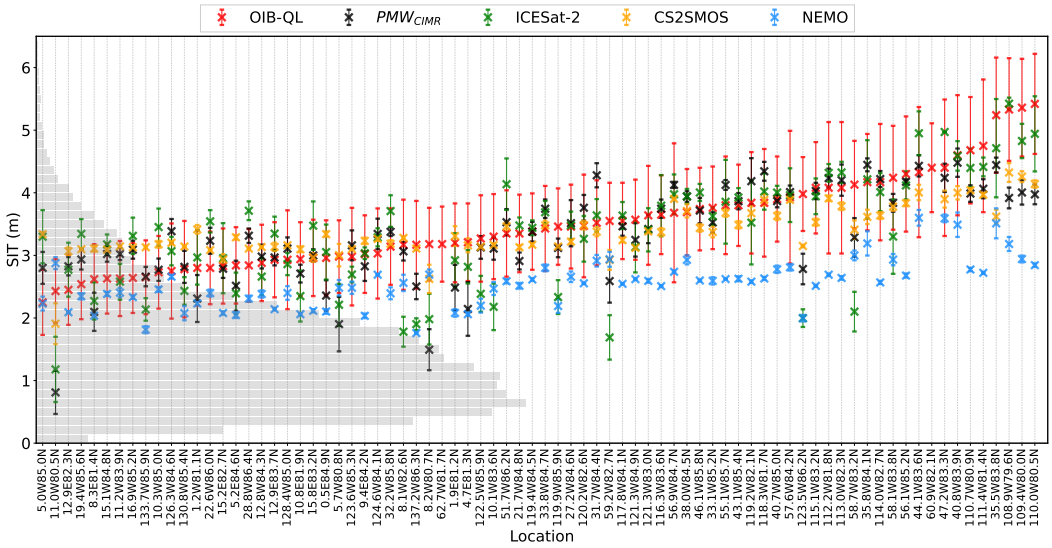

Figure 7. Comparison of SIT measurements from OIB-QL (red), PMW_{CIMR} retrieval (black), ICESat-2 (green), CS2SMOS (orange) and NEMO (blue) products. The error bars represent the mean SIT uncertainty for OIB-QL measurements and one standard deviation for the other SIT estimations. The normalized distribution of the ICESat-2 SIT is shown in grey shades on the left y-axis.

Table 1. Bias, root-mean-square errors, relative root-mean-square errors and Pearson correlation coefficient between the OIB-QL SIT and the others SIT retrievals.

	Mean Difference (m)	RMSE (m)	Relative RMSE (%)	R
PMW_{CIMR}	0.16	0.57	17	0.72
PMW_{1836}	0.28	0.61	18	0.74
IS2	0.17	0.66	20	0.69
CS2SMOS	0.11	0.49	14	0.80
NEMO	0.94	1.09	28	0.69

The SIT distribution of the OIB-QL mission is heavily weighted toward very high SIT values (mainly above 3 m) representing mostly multi-year ice. That does not correspond to the whole Arctic SIT distribution, where first-year ice with lower SIT are dominating (see the gray shades on Figure 4). The conclusions drawn from this evaluation cannot be extended on the validity of the estimates for low SIT. Note that in the SIT range measured by the OIB-QL campaign (mainly above 3 m), the NN retrieval errors with respect to the other satellite products (ICESat-2 or CS2SMOS) were expected to have RMSE $\sim$ 0.6 m, (see Figure 4).

5 Conclusion

A simple and yet efficient statistical approach is developed to estimate the Sea Ice Thickness (SIT) from passive microwave brightness temperatures between 1.4 and 36 GHz.

It is based on the evidence of high absolute correlations between the observed passive microwave brightness temperatures (especially at 36 GHz) and existing available satellite-derived SIT products. The 1.4 to 36 GHz frequency range will be covered by the future CIMR mission to be launched by the end of the 2020's. Using a combination of SMAP and AMSR2 observations, a neural network (NN) inversion is trained on a subset of ICESat-2 SIT product derived from independent laser-altimeter measurements, and the NN SIT is estimated over the Arctic for a full winter season.

The resulting passive microwave NN SIT using all the CIMR frequencies shows a significant correlation with the ICESat-2 SIT data during the whole Arctic winter (0.85) and an identical spatio-temporal correlation with the CS2SMOS SIT product (0.85). The NN inversion using only the 18 and 36 GHz frequencies also performs satisfactorily, over the full SIT range. That would make it possible to calculate long time series of SIT from former passive microwave imagers such as SMM/I and SSMIS back to the end of the 80's, or even from SSMR, launched in 1978, with all these instruments being equipped with radiometers at 18 and 36 GHz, at both V and H polarizations. Note that there are on-going efforts to inter-calibrate all these microwave imagers for climate purposes, and this SIT estimation could benefit from this very long record of high quality T_B at 18 and 36 GHz.

The NN retrievals were compared to OIB-QL measurement campaign performed in 2019. Both NN retrievals (with all frequencies and with 18 and 36 GHz only) show encouraging performances, comparable to the results obtained with the current ICESat-2 or CS2SMOS SIT products, at least for the SIT range (mainly above 3 m) covered by the OIB-QL measurements.

Several satellite-based SIT exist, each with limitations due to their operating frequency or their algorithm assumptions. The CS2SMOS and ICESat-2 SIT products both require a characterization of the snow cover (snow depth and snow density). The use of dual frequency (Ku/Ka) radar altimeters (as in Kwok et al. (2020) or Garnier et al. (2021)) can help reduce the uncertainties related to the snow depth, and the future CRISTAL mission, to be launched approximately at the same time as CIMR, will be equipped with this dual frequency capability (Kern et al., 2020). The passive microwave SIT retrieval proposed here is based on a pragmatic approach. It does not require any ancillary information. It is easy to apply on a daily basis, on past, current, or future observations, providing close-to global Arctic coverage every day over long time records.

Acknowledgments

Clément Soriot is funded through a CNES and Estellus doctoral fellowship.

The work has been partly supported by the CNES TOSCA contract CIMR_SEAICE (4500069758).

We acknowledge Camille Lique, Ghislain Picard, Gille Garric and, Martin Vancoppenolle for their valuable discussions.

References

Aaboe, S., & Down, E. J. (2021). *Product User Manual for the Global Sea-Ice Edge and Type Product* (Tech. Rep.).

Abdalati, W., Zwally, H. J., Bindschadler, R., Csatho, B., Farrell, S. L., Fricker, H. A., ... Webb, C. (2010, May). The ICESat-2 Laser Altimetry Mission. *Proceedings of the IEEE*, *98*(5), 735–751. (Conference Name: Proceedings of the IEEE) doi: 10.1109/JPROC.2009.2034765

Abdalla, S., Abdeh Kolahchi, A., Ablain, M., Adusumilli, S., Aich Bhowmick, S., Alou-Font, E., ... Zlotnicki, V. (2021, July). Altimetry for the future: Building on 25 years of progress. *Advances in Space Research*, *68*(2), 319–363. Retrieved 2022-06-14, from `https://www.sciencedirect.com/science/`

article/pii/S0273117721000594 doi: 10.1016/j.asr.2021.01.022

Aires, F., Chédin, A., Scott, N. A., & Rossow, W. B. (2002, February). A Regularized Neural Net Approach for Retrieval of Atmospheric and Surface Temperatures with the IASI Instrument. *Journal of Applied Meteorology and Climatology*, *41*(2), 144–159. Retrieved 2022-05-09, from https://journals.ametsoc.org/view/journals/apme/41/2/1520-0450_2002_041_0144_arnnaf_2.0.co_2.xml (Publisher: American Meteorological Society Section: Journal of Applied Meteorology and Climatology) doi: 10.1175/1520-0450(2002)041⟨0144:ARNNAF⟩2.0.CO;2

Braakmann-Folgmann, A., & Donlon, C. (2019, September). Estimating snow depth on Arctic sea ice using satellite microwave radiometry and a neural network. *The Cryosphere*, *13*(9), 2421–2438. Retrieved 2021-10-27, from https://tc.copernicus.org/articles/13/2421/2019/ (Publisher: Copernicus GmbH) doi: 10.5194/tc-13-2421-2019

Brodzik, M. J., Billingsley, B., Haran, T., Raup, B., & Savoie, M. H. (2012, June). EASE-Grid 2.0: Incremental but Significant Improvements for Earth-Gridded Data Sets. *ISPRS International Journal of Geo-Information*, *1*(1), 32–45. Retrieved 2021-09-06, from https://www.mdpi.com/2220-9964/1/1/32 doi: 10.3390/ijgi1010032

Chi, J., & Kim, H.-C. (2021, August). Retrieval of daily sea ice thickness from AMSR2 passive microwave data using ensemble convolutional neural networks. *GIScience & Remote Sensing*, *58*(6), 812–830. Retrieved 2022-01-25, from https://doi.org/10.1080/15481603.2021.1943213 doi: 10.1080/15481603.2021.1943213

Comiso, J. C. (1986). Characteristics of Arctic winter sea ice from satellite multispectral microwave observations. *Journal of Geophysical Research: Oceans*, *91*(C1), 975–994. Retrieved from https://agupubs.onlinelibrary.wiley.com/doi/abs/10.1029/JC091iC01p00975 doi: 10.1029/JC091iC01p00975

Comiso, J. C. (1995). SSM/I Sea Ice Concentrations Using the Bootstrap Algorithm. , 53.

Comiso, J. C., Cavalieri, D. J., & Markus, T. (2003, February). Sea ice concentration, ice temperature, and snow depth using AMSR-E data. *IEEE Transactions on Geoscience and Remote Sensing*, *41*(2), 243–252. doi: 10.1109/TGRS.2002.808317

Cybenko, G. (1989, December). Approximation by superpositions of a sigmoidal function. *Mathematics of Control, Signals and Systems*, *2*(4), 303–314. Retrieved 2022-06-14, from https://doi.org/10.1007/BF02551274 doi: 10.1007/BF02551274

Dai, A., Luo, D., Song, M., & Liu, J. (2019, December). Arctic amplification is caused by sea-ice loss under increasing CO2. *Nature Communications*, *10*(1), 121. Retrieved 2021-09-21, from http://www.nature.com/articles/s41467-018-07954-9 doi: 10.1038/s41467-018-07954-9

Donlon, C. (2020). *CIMR Mission Requirements Document v3 | cimr.eu* (Tech. Rep. No. 4). Retrieved 2021-09-03, from https://cimr.eu/mrd_v3

Entekhabi, D., Njoku, E. G., O'Neill, P. E., Kellogg, K. H., Crow, W. T., Edelstein, W. N., ... Van Zyl, J. (2010, May). The Soil Moisture Active Passive (SMAP) Mission. *Proceedings of the IEEE*, *98*(5), 704–716. Retrieved 2021-01-12, from http://ieeexplore.ieee.org/document/5460980/ doi: 10.1109/JPROC.2010.2043918

Entekhabi, D., Yuech, S., & De Lannoy, G. (2014). SMAP Handbook. *JPL Publicatioon*.

Font, J., Camps, A., Borges, A., Martín-Neira, M., Boutin, J., Reul, N., ... Mecklenburg, S. (2010, May). SMOS: The Challenging Sea Surface Salinity Measurement From Space. *Proceedings of the IEEE*, *98*(5), 649–665. Retrieved 2021-07-22, from http://ieeexplore.ieee.org/document/5340531/ doi:

10.1109/JPROC.2009.2033096

Foresee, F. D., & Hagan, M. T. (1997). Gauss-Newton approximation to Bayesian regularization. In *Proceedings of the 1997 International Joint Conference on Neural Networks* (pp. 1930–1935).

Garnier, F., Fleury, S., Garric, G., Bouffard, J., Tsamados, M., Laforge, A., ... Remy, F. (2021, December). Advances in altimetric snow depth estimates using bi-frequency SARAL and CryoSat-2 Ka–Ku measurements. *The Cryosphere*, *15*(12), 5483–5512. Retrieved 2022-01-17, from https://tc.copernicus.org/articles/15/5483/2021/ doi: 10.5194/tc-15-5483-2021

Gasparin, F., Greiner, E., Lellouche, J.-M., Legalloudec, O., Garric, G., Drillet, Y., ... Drévillon, M. (2018, November). A large-scale view of oceanic variability from 2007 to 2015 in the global high resolution monitoring and forecasting system at Mercator Océan. *Journal of Marine Systems*, *187*, 260–276. Retrieved 2022-04-19, from https://www.sciencedirect.com/science/article/pii/S0924796318300113 doi: 10.1016/j.jmarsys.2018.06.015

Hendricks, S., Ricker, R., & Helm, V. (2016). *User Guide - AWI CryoSat-2 Sea Ice Thickness Data Product (v1.2).* Retrieved 2022-04-19, from https://epic.awi.de/id/eprint/41242/1/AWI_cryosat2_user_guide_v1_2_july2016.pdf

Heygster, G., Huntemann, M., Ivanova, N., Saldo, R., & Pedersen, L. T. (2014, July). Response of passive microwave sea ice concentration algorithms to thin ice. In *2014 IEEE Geoscience and Remote Sensing Symposium* (pp. 3618–3621). Quebec City, QC: IEEE. Retrieved 2020-07-08, from http://ieeexplore.ieee.org/document/6947266/ doi: 10.1109/IGARSS.2014.6947266

Imaoka, K., Maeda, T., Kachi, M., Kasahara, M., Ito, N., & Nakagawa, K. (2012). Status of AMSR2 instrument on GCOM-W1. In *Earth observing missions and sensors: Development, implementation, and characterization II* (Vol. 8528, pp. 201–206). SPIE.

Kaleschke, L., Maaß, N., Haas, C., Hendricks, S., Heygster, G., & Tonboe, R. T. (2010, December). A sea-ice thickness retrieval model for 1.4 GHz radiometry and application to airborne measurements over low salinity sea-ice. *The Cryosphere*, *4*(4), 583–592. Retrieved 2020-07-08, from https://tc.copernicus.org/articles/4/583/2010/ doi: 10.5194/tc-4-583-2010

Kaleschke, L., Tian-Kunze, X., Maaß, N., Beitsch, A., Wernecke, A., Miernecki, M., ... Casal, T. (2016, July). SMOS sea ice product: Operational application and validation in the Barents Sea marginal ice zone. *Remote Sensing of Environment*, *180*, 264–273. Retrieved 2022-04-19, from https://www.sciencedirect.com/science/article/pii/S003442571630102X doi: 10.1016/j.rse.2016.03.009

Kern, M., Cullen, R., Berruti, B., Bouffard, J., Casal, T., Drinkwater, M. R., ... Yackel, J. (2020, July). The Copernicus Polar Ice and Snow Topography Altimeter (CRISTAL) high-priority candidate mission. *The Cryosphere*, *14*(7), 2235–2251. Retrieved 2021-01-12, from https://tc.copernicus.org/articles/14/2235/2020/ doi: 10.5194/tc-14-2235-2020

Kilic, L., Prigent, C., Aires, F., Boutin, J., Heygster, G., Tonboe, R. T., ... Donlon, C. (2018). Expected Performances of the Copernicus Imaging Microwave Radiometer (CIMR) for an All-Weather and High Spatial Resolution Estimation of Ocean and Sea Ice Parameters. *Journal of Geophysical Research: Oceans*, *123*(10), 7564–7580. Retrieved 2020-01-08, from https://agupubs.onlinelibrary.wiley.com/doi/abs/10.1029/2018JC014408 doi: 10.1029/2018JC014408

Krasnopolsky, V. M. (2007). Neural network emulations for complex multidimensional geophysical mappings: Applications of neural network techniques to atmospheric and oceanic satellite retrievals and numerical mod-

eling. *Reviews of Geophysics*, *45*(3). Retrieved from https://agupubs.onlinelibrary.wiley.com/doi/abs/10.1029/2006RG000200 (_eprint: https://agupubs.onlinelibrary.wiley.com/doi/pdf/10.1029/2006RG000200) doi: https://doi.org/10.1029/2006RG000200

Kurtz, N., Richter-Menge, J., Farrell, S., Studinger, M., Paden, J., Sonntag, J., & Yungel, J. (2013). IceBridge Airborne Survey Data Support Arctic Sea Ice Predictions. *Eos, Transactions American Geophysical Union*, *94*(4), 41–41. Retrieved 2022-04-20, from https://onlinelibrary.wiley.com/doi/abs/10.1002/2013EO040001 doi: 10.1002/2013EO040001

Kurtz, N. T., & Farrell, S. L. (2011). Large-scale surveys of snow depth on Arctic sea ice from Operation IceBridge. *Geophysical Research Letters*, *38*(20). Retrieved 2021-11-16, from https://onlinelibrary.wiley.com/doi/abs/10.1029/2011GL049216 doi: 10.1029/2011GL049216

Kurtz, N. T., Farrell, S. L., Studinger, M., Galin, N., Harbeck, J. P., Lindsay, R., ... Sonntag, J. G. (2013, July). Sea ice thickness, freeboard, and snow depth products from Operation IceBridge airborne data. *The Cryosphere*, *7*(4), 1035–1056. Retrieved 2020-07-08, from https://tc.copernicus.org/articles/7/1035/2013/ doi: 10.5194/tc-7-1035-2013

Kurtz, N. T., Studinger, M., Harbeck, J., Onana, V.-D.-P., & Farrell, S. (2012). *IceBridge Sea Ice Freeboard, Snow Depth, and Thickness.* Boulder, Colorado USA: NASA Distributed Active Archive Center at the National Snow and Ice Data Center. Retrieved from http://nsidc.org/data/idcsi2.html

Kwok, R. (2018, October). Arctic sea ice thickness, volume, and multiyear ice coverage: losses and coupled variability (1958–2018). *Environmental Research Letters*, *13*(10), 105005. Retrieved 2022-04-08, from https://iopscience.iop.org/article/10.1088/1748-9326/aae3ec doi: 10.1088/1748-9326/aae3ec

Kwok, R., Kacimi, S., Webster, M. A., Kurtz, N. T., & Petty, A. A. (2020). Arctic Snow Depth and Sea Ice Thickness From ICESat-2 and CryoSat-2 Freeboards: A First Examination. *Journal of Geophysical Research: Oceans*, *125*(3), e2019JC016008. Retrieved 2022-02-15, from https://onlinelibrary.wiley.com/doi/abs/10.1029/2019JC016008 doi: 10.1029/2019JC016008

Laxon, S., Peacock, N., & Smith, D. (2003, October). High interannual variability of sea ice thickness in the Arctic region. *Nature*, *425*(6961), 947–950. Retrieved 2022-04-08, from https://www.nature.com/articles/nature02050 (Number: 6961 Publisher: Nature Publishing Group) doi: 10.1038/nature02050

Laxon, S. W., Giles, K. A., Ridout, A. L., Wingham, D. J., Willatt, R., Cullen, R., ... Davidson, M. (2013). CryoSat-2 estimates of Arctic sea ice thickness and volume. *Geophysical Research Letters*, *40*(4), 732–737. Retrieved 2020-07-08, from https://agupubs.onlinelibrary.wiley.com/doi/abs/10.1002/grl.50193 doi: 10.1002/grl.50193

Lee, S.-M., Meier, W. N., Sohn, B.-J., Shi, H., & Gasiewski, A. J. (2021, July). Estimation of Arctic Basin-Scale Sea Ice Thickness From Satellite Passive Microwave Measurements. *IEEE Transactions on Geoscience and Remote Sensing*, *59*(7), 5841–5850. doi: 10.1109/TGRS.2020.3026949

Lindsay, R., & Schweiger, A. (2013). Unified Sea Ice Thickness Climate Data Record, 1947 Onward, Version 1. (Publisher: NSIDC) doi: 10.7265/N5D50JXV

Madec, G., & Team, N. (2008). NEMO ocean engine. Note du Pole de modelisation. *Institut Pierre-Simon Laplace (IPSL)*, 396.

Maeda, T., Taniguchi, Y., & Imaoka, K. (2016, February). GCOM-W1 AMSR2 Level 1R Product: Dataset of Brightness Temperature Modified Using the Antenna Pattern Matching Technique. *IEEE Transactions on Geoscience and Remote Sensing*, *54*(2), 770–782. doi: 10.1109/TGRS.2015.2465170

Markus, T., & Cavalieri, D. J. (2009). The AMSR-E NT2 sea ice concentration algorithm: Its basis and implementation. *Journal of The Remote Sensing Society of Japan*, *29*(1), 216–225. Retrieved from https://www.jstage.jst.go.jp/article/rssj/29/1/29_1_216/_article/-char/ja/ doi: 10.11440/rssj.29.216

Meissner, T., Wentz, F. J., & Le Vine, D. M. (2018, July). The Salinity Retrieval Algorithms for the NASA Aquarius Version 5 and SMAP Version 3 Releases. *Remote Sensing*, *10*(7), 1121. Retrieved 2021-11-04, from https://www.mdpi.com/2072-4292/10/7/1121 doi: 10.3390/rs10071121

Petty, A. A., Kurtz, N. T., Kwok, R., Markus, T., & Neumann, T. A. (2020). Winter Arctic Sea Ice Thickness From ICESat-2 Freeboards. *Journal of Geophysical Research: Oceans*, *125*(5), e2019JC015764. Retrieved 2022-02-15, from https://onlinelibrary.wiley.com/doi/abs/10.1029/2019JC015764 doi: 10.1029/2019JC015764

Petty, A. A., Kurtz, N. T., Kwok, R., Markus, T., Neumann, T. A., & Keeney, N. (2022). ICESat-2 L4 Monthly Gridded Sea Ice Thickness, Version 2. *NASA National Snow and Ice Data Center Distributed Active Archive Center*. Retrieved 2022-03-09, from https://nsidc.org/data/IS2SITMOGR4/versions/2 (Type: dataset) doi: 10.5067/10.5067/OE8BDP5KU30Q

Petty, A. A., Webster, M., Boisvert, L., & Markus, T. (2018, November). The NASA Eulerian Snow on Sea Ice Model (NESOSIM) v1.0: initial model development and analysis. *Geoscientific Model Development*, *11*(11), 4577–4602. Retrieved 2022-04-19, from https://gmd.copernicus.org/articles/11/4577/2018/ doi: 10.5194/gmd-11-4577-2018

Prechelt, L. (2012). Early Stopping — But When? In G. Montavon, G. B. Orr, & K.-R. Müller (Eds.), *Neural Networks: Tricks of the Trade: Second Edition* (pp. 53–67). Berlin, Heidelberg: Springer Berlin Heidelberg. Retrieved from https://doi.org/10.1007/978-3-642-35289-8_5 doi: 10.1007/978-3-642-35289-8_5

Pörtner, H.-O., Roberts, D. C., Masson-Delmotte, V., Zhai, P., Tignor, M., Poloczanska, E., & Weyer, N. (2019). The ocean and cryosphere in a changing climate. *IPCC Special Report on the Ocean and Cryosphere in a Changing Climate*.

Ricker, R., Hendricks, S., Helm, V., Skourup, H., & Davidson, M. (2014, August). Sensitivity of CryoSat-2 Arctic sea-ice freeboard and thickness on radar-waveform interpretation. *The Cryosphere*, *8*(4), 1607–1622. Retrieved 2020-01-08, from http://www.the-cryosphere.net/8/1607/2014/tc-8-1607-2014.html doi: https://doi.org/10.5194/tc-8-1607-2014⟨https://doi.org/10.5194/tc-8-1607-2014⟩

Ricker, R., Hendricks, S., Kaleschke, L., Tian-Kunze, X., King, J., & Haas, C. (2017, July). A weekly Arctic sea-ice thickness data record from merged CryoSat-2 and SMOS satellite data. *Cryosphere*, *11*(4), 1607–1623. Retrieved 2020-01-08, from http://www.the-cryosphere.net/11/1607/2017/ doi: https://doi.org/10.5194/tc-11-1607-2017

Rodríguez-Fernández, N., de Rosnay, P., Albergel, C., Richaume, P., Aires, F., Prigent, C., & Kerr, Y. (2019, January). SMOS Neural Network Soil Moisture Data Assimilation in a Land Surface Model and Atmospheric Impact. *Remote Sensing*, *11*(11), 1334. Retrieved 2022-04-20, from https://www.mdpi.com/2072-4292/11/11/1334 (Number: 11 Publisher: Multidisciplinary Digital Publishing Institute) doi: 10.3390/rs11111334

Rostosky, P., Spreen, G., Farrell, S. L., Frost, T., Heygster, G., & Melsheimer, C. (2018). Snow Depth Retrieval on Arctic Sea Ice From Passive Microwave Radiometers—Improvements and Extensions to Multiyear Ice Using Lower Frequencies. *Journal of Geophysical Research: Oceans*, *123*(10), 7120–7138. Retrieved 2020-12-02, from https://agupubs.onlinelibrary.wiley.com/doi/

abs/10.1029/2018JC014028 doi: https://doi.org/10.1029/2018JC014028

Rousset, C., Vancoppenolle, M., Madec, G., Fichefet, T., Flavoni, S., Barthélemy, A., ... Vivier, F. (2015). The Louvain-La-Neuve sea ice model LIM3.6: global and regional capabilities. *Geoscientific Model Development*, *8*, 2991– 3005. Retrieved 2021-01-20, from https://hal.archives-ouvertes.fr/hal-01234098 (Publisher: European Geosciences Union) doi: 10.5194/gmd-8-2991-2015

Rumelhart, D. E., Hinton, G. E., & Williams, R. J. (1985). Learning Internal Representations by Error Propagation.
(Section: Technical Reports)

Rösel, A., Kaleschke, L., & Birnbaum, G. (2012, April). Melt ponds on Arctic sea ice determined from MODIS satellite data using an artificial neural network. *The Cryosphere*, *6*(2), 431–446. Retrieved 2021-03-01, from https://tc.copernicus.org/articles/6/431/2012/ doi: 10.5194/tc-6-431-2012

Sallila, H., Farrell, S. L., McCurry, J., & Rinne, E. (2019, April). Assessment of contemporary satellite sea ice thickness products for Arctic sea ice. *The Cryosphere*, *13*(4), 1187–1213. Retrieved 2022-03-28, from https://tc.copernicus.org/articles/13/1187/2019/ doi: 10.5194/tc-13-1187-2019

Schutz, B. E., Zwally, H. J., Shuman, C. A., Hancock, D., & DiMarzio, J. P. (2005). Overview of the ICESat Mission. *Geophysical Research Letters*, *32*(21). Retrieved 2022-04-11, from https://onlinelibrary.wiley.com/doi/abs/10.1029/2005GL024009 doi: 10.1029/2005GL024009

Serreze, M. C., & Barry, R. G. (2011, May). Processes and impacts of Arctic amplification: A research synthesis. *Global and Planetary Change*, *77*(1), 85–96. Retrieved 2022-05-11, from https://www.sciencedirect.com/science/article/pii/S0921818111000397 doi: 10.1016/j.gloplacha.2011.03.004

Shi, L., Allen, C. T., Ledford, J. R., Rodriguez-Morales, F., Blake, W. A., Panzer, B. G., ... Gogineni, S. (2010, July). Multichannel Coherent Radar Depth Sounder for NASA Operation Ice Bridge. In *2010 IEEE International Geoscience and Remote Sensing Symposium* (pp. 1729–1732). (ISSN: 2153-7003) doi: 10.1109/IGARSS.2010.5649518

Soriot, C., Picard, G., Prigent, C., Frappart, F., & Domine, F. (2022, September). Year-round sea ice and snow characterization from combined passive and active microwave observations and radiative transfer modeling. *Remote Sensing of Environment*, *278*, 113061. Retrieved 2022-05-18, from https://www.sciencedirect.com/science/article/pii/S0034425722001754 doi: 10.1016/j.rse.2022.113061

Stroeve, J. C., Serreze, M. C., Holland, M. M., Kay, J. E., Malanik, J., & Barrett, A. P. (2012, February). The Arctic's rapidly shrinking sea ice cover: a research synthesis. *Climatic Change*, *110*(3-4), 1005–1027. Retrieved 2022-05-17, from http://link.springer.com/10.1007/s10584-011-0101-1 doi: 10.1007/s10584-011-0101-1

Tian-Kunze, X., Kaleschke, L., Maaß, N., Mäkynen, M., Serra, N., Drusch, M., & Krumpen, T. (2014, May). SMOS-derived thin sea ice thickness: algorithm baseline, product specifications and initial verification. *The Cryosphere*, *8*(3), 997–1018. Retrieved 2021-02-09, from https://tc.copernicus.org/articles/8/997/2014/ doi: 10.5194/tc-8-997-2014

Tilling, R. L., Ridout, A., & Shepherd, A. (2018, September). Estimating Arctic sea ice thickness and volume using CryoSat-2 radar altimeter data. *Advances in Space Research*, *62*(6), 1203–1225. Retrieved 2022-01-11, from https://www.sciencedirect.com/science/article/pii/S0273117717307901 doi: 10.1016/j.asr.2017.10.051

Tonboe, R. T., Lavelle, J., Pfeiffer, R.-H., & Howe, E. (2017). *Product User Manual for OSI SAF Global Sea Ice Concentration* (Tech. Rep.). EUMETSAT. Retrieved 2021-09-06, from http://osisaf.met.no/docs/

osisaf_cdop3_ss2_pum_ice-conc_v1p5.pdf

Ulaby, F., & Long, D. G. (2014). *Microwave Radar and Radiometric Remote Sensing*. The University of Michigan Press.

Verron, J., Sengenes, P., Lambin, J., Noubel, J., Steunou, N., Guillot, A., ... Gupta, P. K. (2015, September). The SARAL/AltiKa Altimetry Satellite Mission. *Marine Geodesy*, *38*(sup1), 2–21. Retrieved 2020-10-06, from https://www.tandfonline.com/doi/full/10.1080/01490419.2014.1000471 doi: 10.1080/01490419.2014.1000471

Walker, N. P., Partington, K. C., Van Woert, M. L., & Street, T. L. T. (2006, December). Arctic Sea Ice Type and Concentration Mapping Using Passive and Active Microwave Sensors. *IEEE Transactions on Geoscience and Remote Sensing*, *44*(12), 3574–3584. Retrieved 2021-09-21, from http://ieeexplore.ieee.org/document/4014329/ doi: 10.1109/TGRS.2006.881116

Wang, X., Key, J., Kwok, R., & Zhang, J. (2016, September). Comparison of Arctic Sea Ice Thickness from Satellites, Aircraft, and PIOMAS Data. *Remote Sensing*, *8*(9), 713. Retrieved 2022-04-11, from https://www.mdpi.com/2072-4292/8/9/713 (Number: 9 Publisher: Multidisciplinary Digital Publishing Institute) doi: 10.3390/rs8090713

Warren, S. G., Rigor, I. G., Untersteiner, N., Radionov, V. F., Bryazgin, N. N., & Aleksandrov, Y. I. (1999). Snow Depth on Arctic Sea Ice. *JOURNAL OF CLIMATE*, *12*, 16.

Wingham, D., Rapley, C., & Griffiths, H. (1986). New techniques in satellite altimeter tracking systems. In *Proceedings of IGARSS* (Vol. 86, pp. 1339–1344).